Journal of Information Systems Engineering and Management
2026, 11(3s)
e-ISSN: 2468-4376
https://www.jisem-journal.com/

Research Article

Hybrid Wavelet and K-Means Clustering Framework with Bilateral Filtering for Automated COVID-19 CT Lesion Segmentation

Gul Filiz Tchoketch Kebir [1], Messaouda Larbi[1] Abdelghani Rouini [2] And Mieriem Lina Obeidi[1]
[1] *Department of Computer Science, University of Ziane Achour of Djelfa, 17000, Algeria*
[2] *Laboratory of Computer Science, Mathematics, Automation and Artificial Intelligence (LIMAIA), University of Ziane Achour of Djelfa, 17000, Algeria*
**Corresponding Author: larbi_messaouda@yahoo.fr*

ARTICLE INFO

Received: 05 April 2025

Revised: 07 Oct 2025

Accepted: 15 April 2026

ABSTRACT

Coronavirus disease (COVID-19) has emerged as a major global health challenge, making early and accurate diagnosis crucial, particularly for asymptomatic patients. Computed Tomography (CT) imaging has proven to be an effective modality for detecting COVID-19-related lung abnormalities.

In this paper, a hybrid framework integrating Wavelet Transform (WT), K-Means Clustering (K-MC), and Bilateral Filtering (BF) is proposed for automated segmentation of COVID-19 lesions in chest CT images. Initially, WT is employed for image denoising in the frequency domain to suppress noise while preserving structural details. Subsequently, K-Means clustering based on texture characteristics and local gray-level entropy is applied to achieve automatic segmentation of infected regions. The obtained segmentation results are further refined using bilateral filtering to reduce residual noise and preserve edge information. Finally, morphological post-processing operations are performed to improve segmentation accuracy and region consistency.

Experimental results obtained on a publicly available COVID-19 CT dataset demonstrate that the proposed framework achieves a mean Dice coefficient of 0.8177, a Jaccard index of 0.7322, a sensitivity of 0.8281, a precision of 0.8538, and a specificity of 0.9837. Furthermore, the proposed method outperforms four state-of-the-art segmentation approaches (CV, MAC, FRAGL, and SPF) while reducing computational time by more than 87% compared with conventional methods. These findings highlight the effectiveness and computational efficiency of the proposed framework for automated COVID-19 CT image analysis.

Keywords: COVID-19, computed tomography, image segmentation, K-means clustering, wavelet transform, bilateral filtering, lung infection.

INTRODUCTION

Coronavirus disease 2019 (COVID-19), caused by the novel severe acute respiratory syndrome coronavirus 2 (SARS-CoV-2), has rapidly evolved into a major global health crisis [1–3]. Early and accurate diagnosis remains crucial for controlling disease transmission and enabling timely clinical intervention. Reverse Transcription Polymerase Chain Reaction (RT-PCR) is widely recognized as the standard diagnostic technique for detecting COVID-19 infection [2]. However, RT-PCR testing requires labor-intensive laboratory procedures performed under strictly controlled conditions and often involves relatively long processing times. In addition, false-negative RT-PCR results may delay treatment and increase the risk of viral transmission [3].

Medical imaging has emerged as an efficient and reliable complementary diagnostic tool for COVID-19 detection. In particular, Computed Tomography (CT) imaging plays an important role in identifying suspected and asymptomatic cases, especially in patients showing rapid progression toward viral pneumonia and severe pulmonary infections. Previous studies have demonstrated that CT imaging may provide higher sensitivity than RT-PCR for detecting

Journal of Information Systems Engineering and Management
2026, 11(3s)
e-ISSN: 2468-4376
https://www.jisem-journal.com/

Research Article

COVID-19-related lung abnormalities [4]. Consequently, automatic localization and segmentation of infected lung regions can significantly assist radiologists in clinical interpretation and decision-making processes [4,5].

Image segmentation represents a fundamental task in medical image analysis. Its primary objective is to isolate regions of interest (ROIs) from surrounding tissues while facilitating the extraction of meaningful features such as texture, intensity, and shape [6–8]. With the rapid advancement of medical imaging technologies, an enormous volume of medical images is generated daily. Manual segmentation of these datasets is time-consuming, subjective, and often impractical in clinical environments. Therefore, the development of automatic and reliable medical image segmentation techniques has become a major research challenge.

Segmentation of CT images remains particularly challenging due to heterogeneous tissue characteristics, unclear boundaries, noise, and complex anatomical structures [9]. Over the past decades, numerous segmentation approaches have been proposed for CT image analysis [10]. Among these methods, clustering-based techniques have demonstrated promising performance in medical image classification and segmentation tasks [11,12]. Such methods rely on similarity and dissimilarity measures between grayscale pixel intensities and are generally categorized into thresholding-based, fuzzy-based, and clustering-based approaches [12].

K-Means Clustering (K-MC) is one of the most widely used clustering algorithms for medical image segmentation. It assigns each pixel to a specific cluster according to distance measurements, making it suitable for grayscale image analysis and segmentation tasks [13–15]. In parallel, Wavelet Transform (WT) techniques have gained considerable attention in medical image processing because of their ability to perform multi-resolution analysis and effective noise reduction [16]. For example, Mohsen et al. combined principal component analysis, discrete wavelet transform, and deep learning techniques for tumor detection; however, their study was limited to brain MRI images [17].

Despite the significant progress achieved in CT image segmentation, many existing approaches are designed for specific applications and often suffer from limited generalization capability. Deep learning-based methods usually provide high segmentation accuracy but require large annotated datasets and extensive computational resources, which restrict their applicability in resource-constrained clinical environments [4,5]. On the other hand, traditional unsupervised approaches, including active contour models [32,33] and region-based methods [34,35], are often computationally expensive and highly sensitive to image noise.

To address these limitations, this paper proposes a hybrid Wavelet-based K-Means clustering framework enhanced with Bilateral Filtering (BF) for automated segmentation of COVID-19 lesions in chest CT images. The proposed framework combines multi-resolution wavelet denoising, unsupervised K-Means clustering, and edge-preserving bilateral filtering to achieve accurate and fully automatic segmentation without requiring annotated training data. In addition, the proposed approach aims to reduce computational complexity while preserving important structural information in CT images.

The main contributions of this work are summarized as follows:

• A hybrid segmentation framework integrating Wavelet Transform, K-Means Clustering, and Bilateral Filtering is proposed for automated COVID-19 CT image analysis.

• The proposed framework performs accurate lesion segmentation without requiring annotated training datasets or computationally intensive learning procedures.

• The proposed method is evaluated using publicly available COVID-19 CT datasets and compared with several state-of-the-art segmentation techniques using standard quantitative evaluation metrics.

• Experimental results demonstrate that the proposed framework achieves competitive segmentation accuracy while significantly reducing computational time.

MATERIALS AND EVALUATION METRICS

A. CT Image Dataset

Journal of Information Systems Engineering and Management
2026, 11(3s)
e-ISSN: 2468-4376
https://www.jisem-journal.com/

Research Article

Chest X-ray imaging is widely used in clinical practice for diagnosing COVID-19 pneumonia [18]. However, Computed Tomography (CT) imaging provides higher visibility and more detailed anatomical information compared with chest X-ray images. Therefore, CT images were adopted in this study for experimental evaluation.

To assess the performance of the proposed segmentation framework, a publicly available COVID-19 CT image dataset was utilized [19]. The dataset consists of 100 chest CT images with a spatial resolution of 512 × 512 pixels. Each image is associated with a corresponding ground-truth segmentation mask, which was used as a reference annotation for quantitative performance evaluation.

B. Evaluation Metrics

To quantitatively evaluate the performance of the proposed segmentation framework, several widely used evaluation metrics were employed, including:

- Dice Similarity Coefficient (DSC)
- Jaccard Index (IoU)
- Precision
- Sensitivity (Recall)
- Specificity
- Matthews Correlation Coefficient (MCC)
- Computational time and number of iterations

These metrics were computed by comparing the predicted segmentation results with the corresponding ground-truth masks.

Let TP, TN, FP, and FN denote True Positive, True Negative, False Positive, and False Negative pixels, respectively

a. Dice Similarity Coefficient (DSC)

The Dice Similarity Coefficient is one of the most commonly used evaluation metrics in medical image segmentation [20]. It measures the degree of overlap between the predicted segmentation and the corresponding ground-truth mask. In addition, it is widely used for assessing the reproducibility of manual annotations [21].

$$Dice = \frac{2TP}{2TP + FP + FN} \quad (1)$$

b. Jaccard Index (IoU)

The Jaccard Index evaluates the similarity between the predicted segmentation and the ground truth by dividing the intersection area by the union area of both regions [22].

$$Jaccard = \frac{TP}{TP + FP + FN} \quad (2)$$

c. Precision (Positive Predictive Value)

Precision, also known as Positive Predictive Value (PPV), measures the proportion of correctly predicted positive pixels among all predicted positive pixels.

$$Precision = \frac{TP}{TP + FP} \quad (3)$$

Journal of Information Systems Engineering and Management
2026, 11(3s)
e-ISSN: 2468-4376
https://www.jisem-journal.com/

Research Article

d. Sensitivity (Recall)

Sensitivity measures the proportion of actual infected pixels that are correctly identified by the segmentation algorithm [23].

$$Sensitivity = \frac{TP}{TP + FN} \qquad (4)$$

e. Matthews Correlation Coefficient (MCC)

The Matthews Correlation Coefficient evaluates the correlation between predicted labels and ground-truth annotations [24]. Unlike conventional metrics, MCC provides a balanced evaluation even in the presence of class imbalance.

$$MCC = \frac{TP \times TN - FP \times FN}{\sqrt{(TP+FP)(TP+FN)(TN+FP)(TN+FN)}} \qquad (5)$$

The MCC value ranges from −1 to 1, where:

1 indicates perfect prediction

0 indicates random prediction

−1 indicates complete disagreement

f. Specificity

Specificity measures the proportion of correctly identified negative pixels [23]

$$Specificity = \frac{TN}{TN + FP} \qquad (6)$$

PREREQUISITES FOR THE PROPOSED METHOD

This study aims to automatically segment COVID-19 infection regions from chest CT images. To achieve this objective, a hybrid image segmentation framework is proposed to improve segmentation accuracy while reducing noise and image irregularities commonly present in CT scans.

The proposed framework consists of three main stages:

1. Wavelet-based image denoising using Discrete Wavelet Transform (DWT)
2. Image segmentation using K-Means Clustering (K-MC)
3. Segmentation refinement using Bilateral Filtering (BF)

First, DWT is applied as a preprocessing step to suppress noise while preserving important structural details in CT images. Subsequently, K-Means clustering is employed to automatically segment infected lung regions based on pixel intensity distribution and texture characteristics. Finally, bilateral filtering is utilized to refine segmentation boundaries and reduce residual artifacts while preserving edge information.

The overall workflow of the proposed framework is illustrated in Fig. 1.

Journal of Information Systems Engineering and Management
2026, 11(3s)
e-ISSN: 2468-4376
https://www.jisem-journal.com/

Research Article

Figure 1. Block diagram of the proposed method.

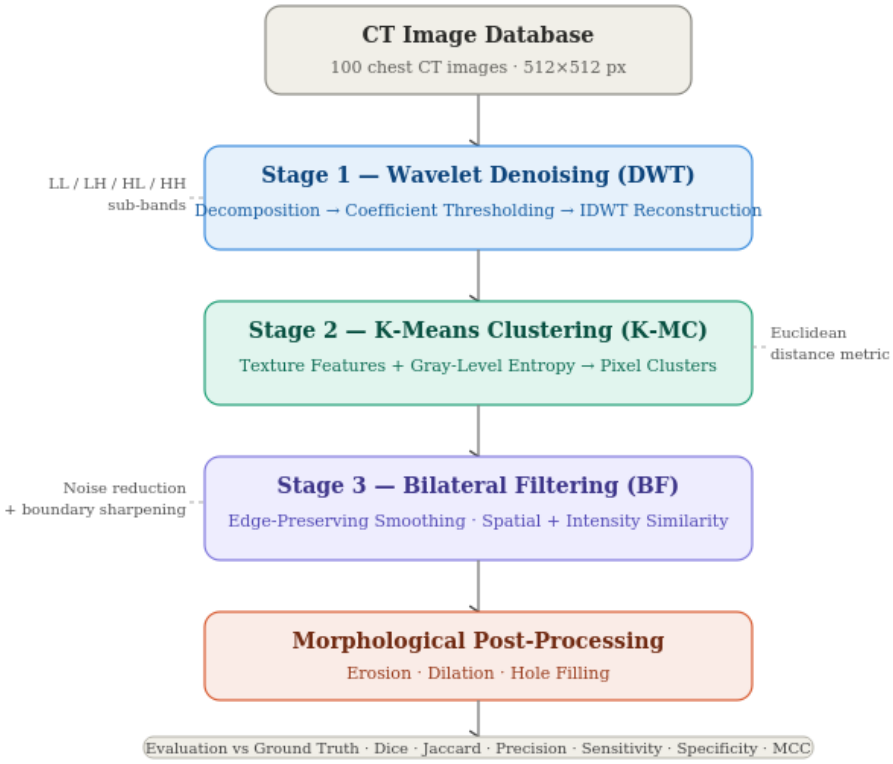

C. Wavelet Transform for Image Denoising

Medical images are often affected by noise and intensity irregularities that may degrade segmentation accuracy. Therefore, noise reduction is performed as a preprocessing stage using the Discrete Wavelet Transform (DWT).

The wavelet-based denoising procedure consists of three main steps:

•Wavelet decomposition

•Thresholding of wavelet coefficients

•Image reconstruction using the Inverse Discrete •Wavelet Transform (IDWT)

DWT provides multi-resolution analysis, allowing the image to be analyzed at different frequency bands and spatial resolutions. This characteristic makes wavelet transforms particularly suitable for medical image denoising applications.

During decomposition, the CT image is divided into four frequency sub-bands:

•Low-frequency approximation coefficients (LL)

•Horizontal detail coefficients (LH)

•Vertical detail coefficients (HL)

•Diagonal detail coefficients (HH)

The LL sub-band contains coarse structural information, Whereas the remaining sub-bands preserve edge and high-frequency image details [25].

Let $\psi(t)$denote the mother wavelet satisfying the admissibility condition [26]. A family of wavelets can be generated through scaling and translation operations:

Journal of Information Systems Engineering and Management
2026, 11(3s)
e-ISSN: 2468-4376
https://www.jisem-journal.com/

Research Article

$$\psi_{p,q}(t) = \frac{1}{\sqrt{p}}\psi\left(\frac{t-q}{p}\right) \quad (7)$$

Where $p$and $q$represent the scaling and translation parameters, respectively.

A two-dimensional wavelet decomposition of a CT image $I(x,y)$at decomposition level $i$can be expressed as:

$$W_i = \{LL_i, LH_i, HL_i, HH_i\} \quad (8)$$

This decomposition process effectively suppresses noise while preserving important structural information required for accurate segmentation.

D. K-Means Clustering for Image Segmentation

After the denoising stage, image segmentation is performed using the K-Means Clustering (K-MC) algorithm. K-Means is an unsupervised clustering technique widely used in medical image segmentation because of its simplicity, efficiency, and low computational complexity [27–29].

The main objective of clustering is to group pixels with similar intensity characteristics into homogeneous regions. Let the dataset consist of $v$observations represented by f-dimensional feature vectors. K-Means partitions the dataset into $m$clusters by minimizing the intra-cluster distance between data points and their corresponding centroids.

The K-Means clustering procedure can be summarized as follows:

1. Randomly initialize $m$cluster centroids
2. Assign each pixel to the nearest centroid using Euclidean distance
3. Update cluster centroids by averaging the assigned cluster members
4. Repeat the process until convergence is achieved

This stage produces the initial segmentation of infected lung regions from chest CT images.

E. Bilateral Filtering for Segmentation Refinement

Although K-Means clustering produces effective segmentation results, the segmented boundaries may still contain noise and irregular artifacts. To improve boundary quality and segmentation consistency, Bilateral Filtering (BF) is applied as a post-processing step.

The bilateral filter performs image smoothing while preserving important edge information, making it particularly suitable for medical image enhancement applications. Unlike conventional smoothing filters, bilateral filtering simultaneously considers:

• Spatial proximity

• Intensity similarity

This property enables smoothing within homogeneous regions while preserving boundaries between different anatomical tissues.

The output of the bilateral filter at pixel $s$is defined as follows [30–31]:

$$I'(s) = \frac{1}{k(s)}\sum_{p\in\Omega} I(p)\ f_r(|\ I(p) - I(s)\ |)\ f_d(|\ p - s\ |) \quad (9)$$

Where $k(s)$denotes the normalization factor:

$$k(s) = \sum_{p\in\Omega} f_r\ (|\ I(p) - I(s)\ |)\ f_d(|\ p - s\ |) \quad (10)$$

Journal of Information Systems Engineering and Management
2026, 11(3s)
e-ISSN: 2468-4376
https://www.jisem-journal.com/

Research Article

This refinement stage removes residual noise and improves the boundary accuracy of the segmented COVID-19 infection regions.

RESULTS AND DISCUTIONS

This section presents the experimental evaluation of the proposed segmentation framework in terms of quantitative performance and visual quality. The proposed approach is compared with several state-of-the-art segmentation methods, including CV [32], MAC [33], FRAGL [34], and SPF [35].

All experiments were conducted using MATLAB R2018a (64-bit) on a Windows 7 workstation equipped with an Intel Core i7 processor operating at 4 GHz and 8 GB RAM. Twelve CT images selected from the COVID-19 dataset [19] were used for performance evaluation. Although the quantitative evaluation was conducted on twelve representative CT images, the selected samples include different infection patterns and varying lesion distributions to ensure robust performance assessment.

A. Visual Evaluation

Figure 2 illustrates the qualitative segmentation results obtained using the proposed framework and the competing segmentation approaches. Visual analysis indicates that several existing methods fail to accurately delineate infection boundaries and often suffer from leakage artifacts and noise within segmented regions.

In contrast, the proposed hybrid framework provides more accurate delineation of infected lung regions while preserving important structural details and reducing segmentation artifacts. These improvements are mainly attributed to the combined effect of wavelet-based denoising, clustering-based segmentation, and bilateral filtering refinement.

Furthermore, the proposed method demonstrates improved robustness in handling heterogeneous infection textures and unclear boundaries commonly observed in COVID-19 chest CT images.

B. Quantitative Evaluation

The quantitative performance of all evaluated methods is summarized in Table 1 using the following evaluation metrics:

- Dice Similarity Coefficient (DSC)
- Jaccard Index (IoU)
- Precision
- Sensitivity
- Specificity
- Matthews Correlation Coefficient (MCC)
- Computational time

The experimental results clearly demonstrate the effectiveness and superiority of the proposed framework compared with the competing segmentation approaches.

The proposed method achieves the highest performance across most evaluation metrics, indicating stronger agreement with the ground-truth annotations. In particular:

- Higher Dice and Jaccard scores indicate improved segmentation accuracy and overlap performance.
- Increased precision and sensitivity demonstrate more reliable detection of infected lung regions.
- Higher MCC values confirm stronger consistency with the reference annotations.
- Reduced computational time highlights the efficiency and practical applicability of the proposed framework.

Journal of Information Systems Engineering and Management
2026, 11(3s)
e-ISSN: 2468-4376
https://www.jisem-journal.com/

Research Article

The reduced computational complexity is mainly attributed to the unsupervised nature of K-Means clustering and the absence of computationally intensive training procedures.

Among the compared methods, the SPF approach achieved the second-best overall performance, whereas the remaining methods produced lower segmentation accuracy and higher computational cost.

The obtained results demonstrate stable segmentation performance across different CT images, indicating the robustness and consistency of the proposed framework under varying lesion characteristics and image conditions.

C. Discussion

The superior performance of the proposed framework can be attributed to the complementary strengths of its three main components:

1. Wavelet Transform effectively suppresses image noise while preserving important structural information.
2. K-Means Clustering provides efficient and computationally simple initial segmentation of infected lung tissues.
3. Bilateral Filtering refines segmentation boundaries and removes residual artifacts while preserving edge information.

Moreover, the proposed framework effectively preserves important edge and texture information, which is essential for accurate delineation of COVID-19 infection regions.

The integration of these techniques enables robust segmentation performance even in challenging CT images characterized by heterogeneous textures, low contrast, and unclear anatomical boundaries.

In addition, unlike deep learning-based approaches, the proposed framework does not require annotated training datasets or computationally intensive training procedures, making it more suitable for resource-constrained clinical environments.

Overall, the experimental results confirm that the proposed framework provides a reliable, accurate, and computationally efficient solution for automated COVID-19 CT image segmentation.

Journal of Information Systems Engineering and Management
2026, 11(3s)
e-ISSN: 2468-4376
https://www.jisem-journal.com/

Research Article

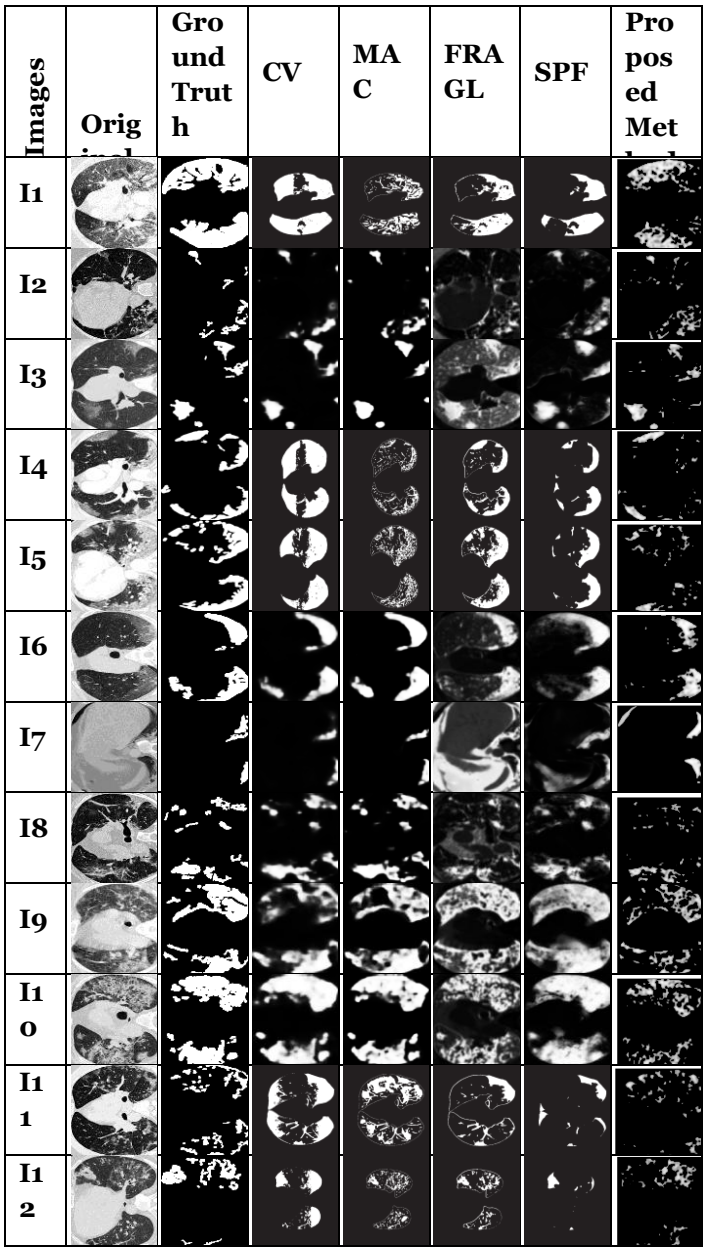

Figure 2. Outcomes of all proposed models in terms of the database.

Journal of Information Systems Engineering and Management
2026, 11(3s)
e-ISSN: 2468-4376
https://www.jisem-journal.com/

Research Article

Images	Metrics	CV	MAC	FRAGL	SPF	Proposed Method
I1	Time (s)	104	165	170	210	14.7602
	Sensitivity	0.6501	0.6664	0.6836	0.7485	0.7321
	Precision	0.9365	0.9465	0.8851	0.7138	0.9644
	MCC	0.8296	0.8492	0.7631	0.7750	0.8484
	Dice	0.8494	0.8372	0.7941	0.7543	0.8601
	Jaccard	0.6585	0.6349	0.6319	0.7318	0.8388
	Specificity	0.9832	0.8856	0.7830	0.8931	0.9844
I2	Time (s)	170	160	200	190	20.6729
	Sensitivity	0.6666	0.7577	0.6565	0.7882	0.9163
	Precision	0.6588	0.7875	0.4137	0.6163	0.7773
	MCC	0.6450	0.7095	0.4300	0.3614	0.7307
	Dice	0.6164	0.7849	0.5212	0.7310	0.7401
	Jaccard	0.5776	0.6563	0.3568	0.5635	0.5822
	Specificity	0.8854	0.9747	0.9562	0.8902	0.9960
I3	Time (s)	130	165	190	60	18.6662
	Sensitivity	0.7313	0.7598	0.7578	0.8964	0.9002
	Precision	0.8810	0.7229	0.6006	0.8815	0.8140
	MCC	0.6609	0.7001	0.5111	0.7177	0.8765
	Dice	0.6100	0.7410	0.6585	0.8549	0.8665
	Jaccard	0.5806	0.7356	0.5435	0.7666	0.7829
	Specificity	0.8441	0.9522	0.9391	0.9371	0.9549
I4	Time (s)	166	187	220	60	24.4575
	Sensitivity	0.5542	0.6719	0.6830	0.7820	0.6910
	Precision	0.6487	0.7800	0.7126	0.8502	0.8200
	MCC	0.6942	0.7261	0.6715	0.7399	0.7576
	Dice	0.6989	0.7719	0.7274	0.7533	0.7788
	Jaccard	0.5123	0.5578	0.5310	0.6673	0.7100
	Specificity	0.8987	0.8823	0.8671	0.8874	0.9761
I5	Time (s)	170	177	199	75	23.8499
	Sensitivity	0.7955	0.7932	0.7533	0.8493	0.8952
	Precision	0.8141	0.9538	0.7698	0.8934	0.9337
	MCC	0.8758	0.8773	0.7868	0.8888	0.8716
	Dice	0.8585	0.7771	0.7925	0.6139	0.8750
	Jaccard	0.8733	0.8971	0.7842	0.8534	0.8816
	Specificity	0.9026	0.9528	0.9263	0.9507	0.9770
I6	Time (s)	170	174	150	80	23.9660
	Sensitivity	0.7403	0.8788	0.8500	0.7526	0.9179
	Precision	0.8009	0.7118	0.7350	0.8296	0.8820
	MCC	0.7530	0.7620	0.7133	0.4983	0.7685
	Dice	0.8401	0.8497	0.8186	0.7212	0.8547
	Jaccard	0.7423	0.7617	0.6229	0.7496	0.7462
	Specificity	0.8253	0.8314	0.8023	0.9404	0.9557
I7	Time (s)	180	160	170	87	19.8066
	Sensitivity	0.6310	0.7200	0.8930	0.8521	0.8945
	Precision	0.5664	0.6325	0.2522	0.7619	0.6349
	MCC	0.5943	0.6710	0.3565	0.6079	0.6771
	Dice	0.5991	0.6744	0.2600	0.6611	0.7383
	Jaccard	0.4210	0.5017	0.1494	0.0601	0.5036
	Specificity	0.9910	0.9900	0.9455	0.8622	0.9977
I8	Time (s)	120	174	182	82	16.8803
	Sensitivity	0.6506	0.7771	0.7126	0.7885	0.7563
	Precision	0.8265	0.8810	0.7561	0.8820	0.9574
	MCC	0.7296	0.8512	0.6661	0.8710	0.8484
	Dice	0.7194	0.8772	0.6745	0.8743	0.7503
	Jaccard	0.8885	0.7910	0.5320	0.6323	0.7398
	Specificity	0.9241	0.9222	0.9720	0.9720	0.9944
I9	Time (s)	150	174	191	72	16.8803
	Sensitivity	0.7506	0.7664	0.6226	0.7385	0.7653
	Precision	0.9265	0.9470	0.7851	0.8138	0.9574
	MCC	0.8196	0.8392	0.6731	0.7540	0.8484
	Dice	0.8294	0.8472	0.6945	0.7743	0.8503
	Jaccard	0.7085	0.7349	0.5319	0.7318	0.8398
	Specificity	0.9941	0.9957	0.9830	0.9831	0.9944
I10	Time (s)	155	171	183	52	16.8803
	Sensitivity	0.7810	0.6664	0.7226	0.7286	0.8153
	Precision	0.8265	0.8470	0.8751	0.9910	0.8974
	MCC	0.8169	0.8491	0.7731	0.7240	0.8484
	Dice	0.8184	0.8672	0.7945	0.8243	0.8503
	Jaccard	0.7885	0.7649	0.5419	0.7318	0.7398
	Specificity	0.9541	0.9857	0.9130	0.9431	0.9944

Table 1. Detailed evaluation of seven metrics based on Covid-19 CT images

Journal of Information Systems Engineering and Management
2026, 11(3s)
e-ISSN: 2468-4376
https://www.jisem-journal.com/

Research Article

CONCLUSION

In this paper, a hybrid framework for automated segmentation of COVID-19 infection regions from chest CT images was proposed. The proposed framework integrates Discrete Wavelet Transform (DWT) for image denoising, K-Means Clustering (K-MC) for initial segmentation, and Bilateral Filtering (BF) for segmentation refinement.

The proposed approach effectively addresses several common challenges associated with CT image segmentation, including image noise, heterogeneous textures, and unclear anatomical boundaries. Experimental evaluation conducted on COVID-19 CT images demonstrated that the proposed framework achieves a mean Dice coefficient of 0.8177, a Jaccard index of 0.7322, a sensitivity of 0.8281, a precision of 0.8538, and a specificity of 0.9837. Furthermore, the proposed method outperformed CV, MAC, FRAGL, and SPF segmentation approaches across most quantitative evaluation metrics.

In addition to segmentation accuracy, the proposed framework demonstrated high computational efficiency, requiring an average processing time of only 19.62 s per image. This represents a computational speedup of more than eight times compared with conventional active contour-based methods.

The combination of wavelet-based preprocessing, clustering-based segmentation, and edge-preserving bilateral filtering enables accurate detection of infected lung regions while maintaining low computational complexity. Moreover, the proposed framework effectively preserves important structural and texture information, which is essential for accurate delineation of COVID-19 lesions.

Overall, the obtained results highlight the potential of the proposed framework as a reliable and computationally efficient computer-aided diagnosis tool for COVID-19 CT image analysis, particularly in resource-constrained clinical environments.

As future work, the proposed framework will be extended to three-dimensional (3D) CT image segmentation and validated using larger and more diverse clinical datasets.

REFRENCES

[1] Paules, C.I.; Marston, H.D.; Fauci, A.S. Coronavirus infections—more than just the common cold. JAMA 2020, 323, 707–708.
[2] Abdelghani ROUINI, Messaouda LARBI, A Neural Network Designed for COVID-19 Detection Using CT Images, Journal of Przegląd doi:10.15199/48.2024.04.29 ISSUE 4, 2024
[3] Gorbalenya, A.E.; Baker, S.C.; Baric, R.S.; de Groot, R.J.; Drosten, C.; Gulyaeva, A.A.; Haagmans, B.L.; Lauber, C.; Leontovich, A.M.; Neuman, B.W.; et al. The species severe acute respiratory syndrome-related coronavirus. Nat. Microbiol. 2020, 5, 536–544.
[4] Wu, Y.H.; Gao, S.H.; Mei, J.; Xu, J.; Fan, D.P.; Zhang, R.G.; Cheng, M.M. JCS: An explainable COVID-19 diagnosis system by joint classification and segmentation. IEEE Trans. Image Process. 2021, 30, 3113–3126.
[5] Abdelghani ROUINI, Messaouda LARBI, A New Approach Of Segmentation Images Based On Wavelet Transform, International Development Planning Review (IDPR)ISSN:1474-6743 | E-ISSN:1478-3401, VOLUME 22 ISSUE 2, 2023.
[6] Chung, M.; Bernheim, A.; Mei, X.; Zhang, N.; Huang, M.; Zeng, X.; Cui, J.; Xu, W.; Yang, Y.; Fayad, Z.A.; et al. CT imaging features of 2019 novel coronavirus (2019-nCoV). Radiology 2020, 295, 202–207.
[7] Abdelghani ROUINI, Messaouda LARBI, Aerial Image Segmentation Using Deep Learning, GRADIVA, ISSN: 0363-8057, VOLUME 63 ISSUE 1, 2024.
[8] Bernheim, A.; Mei, X.; Huang, M.; Yang, Y.; Fayad, Z.A.; Zhang, N.; Diao, K.; Lin, B.; Zhu, X.; Li, K.; et al. Chest CT findings in coronavirus disease-19 (COVID-19): Relationship to duration of infection. Radiology 2020, 295, 200463.
[9] Pan, F.; Ye, T.; Sun, P.; Gui, S.; Liang, B.; Li, L.; Zheng, D.; Wang, J.; Hesketh, R.L.; Yang, L.; et al. Time course of lung changes at chest CT during recovery from coronavirus disease 2019 (COVID-19). Radiology 2020, 295, 715–721.
[10] Li, L.; Qin, L.; Xu, Z.; Yin, Y.; Wang, X.; Kong, B.; Bai, J.; Lu, Y.; Fang, Z.; Song, Q.; et al. Using artificial intelligence to detect COVID-19 and community-acquired pneumonia based on pulmonary CT: Evaluation of the diagnostic accuracy. Radiology 2020, 296, E65–E71.

[11] Shi, F.; Wang, J.; Shi, J.; Wu, Z.; Wang, Q.; Tang, Z.; He, K.; Shi, Y.; Shen, D. Review of artificial intelligence techniques in imaging data acquisition, segmentation, and diagnosis for COVID-19. IEEE Rev. Biomed. Eng. 2021, 14, 4–15.
[12] Xu, R.; Wunsch, D. Survey of clustering algorithms. IEEE Trans. Neural Netw. 2005, 16, 645–678.
[13] Moftah, H.M.; Azar, A.T.; Al-Shammari, E.T.; Ghali, N.I.; Hassanien, A.E.; Shoman, M. Adaptive k-means clustering algorithm for MR breast image segmentation. Neural Comput. Appl. 2014, 24, 1917–1928.
[14] Huang, Y.P.; Singh, P.; Kuo, H.C. A hybrid fuzzy clustering approach for the recognition and visualization of MRI images of Parkinson's disease. IEEE Access 2020, 8, 25041–25051.
[15] Tinnathi, S.; Sudhavani, G. An efficient brain tumor segmentation using adaptive watershed segmentation with AGSO and hybrid feature extraction. J. Vis. Commun. Image Represent. 2021, 74, 102966.
[16] Zhang, L. A medical image segmentation method based on SOM and wavelet transforms. Proc. SPIE 2020, 11429, 114290H.
[17] Mohsen, H.; El-Dahshan, E.S.A.; El-Horbaty, E.S.M.; Salem, A.B.M. Classification using deep learning neural networks for brain tumors. Future Comput. Inform. J. 2018, 3, 68–71.
[18] Rajinikanth, V.; Kadry, S.; Thanaraj, K.P.; Kamalanand, K.; Seo, S. Firefly-algorithm supported scheme to detect COVID-19 lesion in lung CT scan images using Shannon entropy and Markov-random-field. arXiv 2020, arXiv:2004.09239.
[19] Jenssen, H.B. COVID-19 CT Segmentation Dataset. Available online: http://medicalsegmentation.com/covid19/ (accessed on 10 April 2020).
[20] Dice, L.R. Measures of the amount of ecologic association between species. Ecology 1945, 26, 297–302.
[21] Zou, K.H.; Warfield, S.K.; Bharatha, A.; Tempany, C.M.C.; Kaus, M.R.; Haker, S.J.; Wells, W.M.; Jolesz, F.A.; Kikinis, R. Statistical validation of image segmentation quality based on a spatial overlap index. Acad. Radiol. 2004, 11, 178–189.
[22] Jaccard, P. The distribution of the flora in the alpine zone. New Phytol. 1912, 11, 37–50.
[23] Csurka, G.; Larlus, D.; Perronnin, F.; Meylan, F. What is a good evaluation measure for semantic segmentation? In Proceedings of the BMVC, Bristol, UK, 2013; Volume 27.
[24] MAQC Consortium. The MicroArray Quality Control (MAQC)-II study of common practices for the development and validation of microarray-based predictive models. Nat. Biotechnol. 2010, 28, 827–838.
[25] Rai, H.M.; Chatterjee, K. Hybrid adaptive algorithm based on wavelet transform and independent component analysis for denoising of MRI images. Measurement 2019, 144, 72–82.
[26] Mallat, S.G. A theory for multiresolution signal decomposition: the wavelet representation. IEEE Trans. Pattern Anal. Mach. Intell. 1989, 11, 674–693.
[27] Hartigan, J.A. Clustering Algorithms; Wiley: New York, NY, USA, 1975.
[28] Ng, H.P.; Ong, S.H.; Foong, K.W.C.; Goh, P.S.; Nowinski, W.L. Medical image segmentation using k-means clustering and improved watershed algorithm. In Proceedings of the IEEE Southwest Symposium on Image Analysis and Interpretation, Denver, CO, USA, 26–28 March 2006; pp. 61–65.
[29] Vijay, J.; Subhashini, J. An efficient brain tumor detection methodology using K-means clustering algorithm. In Proceedings of the ICCSP, Melmaruvathur, India, 2013; pp. 653–657.
[30] Ono, S.; Miyata, T.; Yamada, I. Cartoon-texture image decomposition using blockwise low-rank texture characterization. IEEE Trans. Image Process. 2014, 23, 1128–1142.
[31] Xu, P.; Wang, W. Improved bilateral texture filtering with edge-aware measurement. IEEE Trans. Image Process. 2018, 27, 3621–3630.
[32] Chan, T.F.; Vese, L.A. Active contours without edges. IEEE Trans. Image Process. 2001, 10, 266–277.
[33] Xie, X.; Mirmehdi, M. MAC: Magnetostatic active contour model. IEEE Trans. Pattern Anal. Mach. Intell. 2008, 30, 632–646.
[34] Ma, D.; Liao, Q.; Chen, Z.; Liao, R.; Ma, H. Adaptive local-fitting-based active contour model for medical image segmentation. Signal Process. Image Commun. 2019, 76, 201–213.
[35] Zhang, K.; Zhang, L.; Song, H.; Zhou, W. Active contours with selective local or global segmentation: A new formulation and level set method. Image Vis. Comput. 2010, 28, 668–676.